Over 20% Efficient CIGS –Perovskite Tandem Solar Cells

Asim Guchhait,[†,#] Herlina Arianita Dewi,[†,#] Shin Woei Leow, [†,#] Hao Wang,[ǂ] Guifang Han,[ǂ] Firdaus Bin Suhaimi,[§] Subodh Mhaisalkar,[†,ǂ,§] Lydia Helena Wong,[†,ǂ,§] and Nripan Mathews[†,ǂ,§]*

[†] Singapore−Berkeley Research Initiative for Sustainable Energy (SinBeRISE), 1 Create Way, Singapore 138602,

[ǂ]Energy Research Institute @ NTU (ERI@N), Nanyang Technological University, Singapore 637553

[§]School of Materials Science & Engineering, Nanyang Technological University, Singapore 639798

Corresponding Author

* Nripan@ntu.edu.sg

Author Contributions

[#] These authors contributed equally to this work

ABSTRACT

The development of high efficiency semi-transparent perovskite solar cells is necessary for application in integrated photovoltaics and tandem solar cells. However, perovskite's sensitivity to temperature and solvents impose a restriction on following processes, thus favouring physical vapor deposition for the transparent contacts. Protection may be necessary especially for high energy sputtering and a transparent buffer layer providing good electrode adhesion and conductivity is desired. Here we evaluate Ag and MoO_x buffer layers in pursuit of high efficiency tandem solar cells. The usage of thin Ag as a buffer layer demonstrated Indium Tin Oxide (ITO) contacts that were resistant to delamination and yielded a 16.0% efficiency of semi-transparent perovskite solar cell with average transparency of 12% in visible range and > 50% in near infra-red. Further application in tandem with Cu(In,Ga)Se showed an overall efficiency of 20.7% in a 4-terminal (4T) configuration exceeding the subcells individual efficiencies.

TOC GRAPHICS

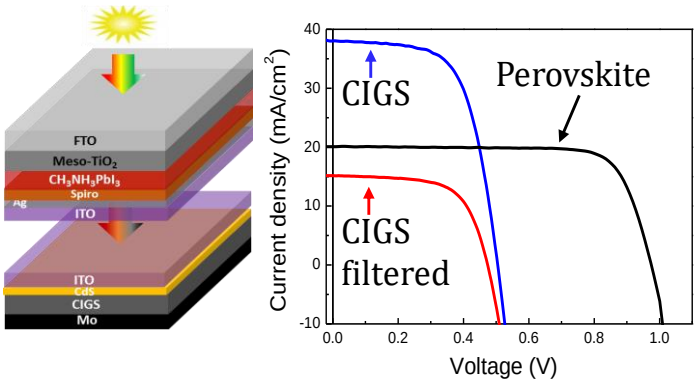

Worldwide adoption of photovoltaics increased exponentially over the last two decades and is expected to become a major source of electrical power in the near future. Development of

integrated photovoltaics will further increase the penetration of photovoltaic technology, and could contribute significantly to the progress of energy neutral buildings. Possessing interesting properties such as long carrier diffusion length, efficient charge transport and tunable colour, in addition to the material's low processing temperature and inexpensive fabrication, perovskite solar cells have been touted as excellent candidates for applications in building integrated photovoltaics (BIPV) and tandem solar cells.[1-6] Rapid progress in perovskite solar cell research has already pushed verified power conversion efficiencies up to 22.1%, far surpassing all other solution-processed photovoltaic technologies.[7-10] However the translation of such high efficiencies to semitransparent perovskite devices necessary for both BIPV and tandem solar cells, requires the development of suitable transparent conducting electrodes which have high transparency, conductivity and process compatibility with prior device fabrication steps is a major concern.

Deposition of transparent conductive oxides (TCO), such as indium tin oxide (ITO), aluminium doped zinc oxide (AZO), or indium zinc oxide (IZO) as an electrode by sputtering, has emerged as a promising method to fabricate semi-transparent devices.[4, 6, 11-14] However, sputter recipes requiring high power may damage the charge transport layers and underlying perovskite layer and thus hampers the device performance.[5, 11, 15] Alternative methods to deposit transparent top electrodes exist, for instance spin coating or mechanically transfer of Ag nanowires, carbon nanotubes and graphene networks.[16-18] Nevertheless these methods are not that robust and reproducible due to possible damage of perovskite by mechanical force or by solvents Hence, the main focus of this work is in the design of sputtering recipes and suitable buffer layers, to preserve semi-transparent device performance without compromising electrode conductivity and transparency.

As it is with the TCO, an ideal buffer layer should exhibit low parasitic absorption, and good compatibility with adjoining layers to ensure proper contact and charge transport.[11, 19] Halide perovskites are known to have solvent and temperature instabilities, as such, low temperature physical vapor deposition processes are preferred. Thermally evaporated molybdenum oxide (MoO_x) and thin Ag are two existing material systems that have been reported as potential buffer layers for semitransparent devices.[5, 11-12, 20] Previous studies on Ag-embedded ITO as an electrode had found that Ag can act as seed layer for crystalline growth of ITO.[20] In the present work, we have performed a comparative study of thin Ag and MoO_x as buffer layers for semi-transparent triple cation perovskite solar cells. We have achieved a PCE efficiency of 16.0% and an average transparency of 54% in the near infrared region using thin Ag. We have applied the semi-transparent cells in a 4-terminal (4T) tandem configuration with Cu(In,Ga)Se (CIGS) cell and attained a tandem efficiency of 20.7%. Although a tandem with Si cells would yield higher efficiency, both Perovskite and CIGS are thin film technologies which are lightweight and can be deposited on flexible substrates. Furthermore, both technologies exhibit radiation hardness and are able to withstand radiation levels several orders higher than crystalline Si, lending them well for high altitudes and space applications.[21-23]

In order to evaluate the utility of Ag and MoO_x as interlayers, bilayer structures of ITO thin films (250 nm) sputtered on 1nm Ag buffer layers and MoO_x were evaluated. Figure 1a and 1b , depicts the optical transparency of the bilayers. Bare ITO is highly transparent with ~80-90% light transmission in the 400-1200nm wavelength range, reaffirming it a suitable TCO candidate. While 1nm evaporated Ag on glass also demonstrates excellent transparency (~80-90%), a combination of 1nm Ag and ITO sees transmission in the visible region fall to ~ 60%, however, near infrared

transmission (>800nm) is unaffected. Increasing Ag thickness from 1 to 3nm could serve to improve ITO crystallinity and sheet resistance, but the payback in transmission losses is severe with only 50% transparency (Figure. S1) in films with 3nm Ag. This is attributed to the formation of non-uniform Ag islands which may cause significant scattering of light. As a compromise between conductivity and light loss, 1nm is chosen as the optimum Ag thickness. From Figure 1b, the transparency of MoO_x at ~80% is better compared to 1nm Ag in the range of 400-700nm, which is within the absorption spectrum of perovskite, thus making it a better choice for bifacial solar cells with regards to light management. Beyond 800 nm, neither Ag nor MoO_x show any significant absorption and the optical absorption of their combined stack defaults to that of ITO, indicating no change in optical properties upon sputtering. Overall transparency for both Ag/ITO and MoO_x/ITO is ~80% in the near infrared region which is transparent to perovskite, making both buffer layers suitable candidates for top electrode for perovskite tandem applications. Higher thicknesses of MoO_x yielded poor device performance (Figure S2). Thinner MoO_x resulted in poor film coverage and may have offered little protection against damage during sputtering.

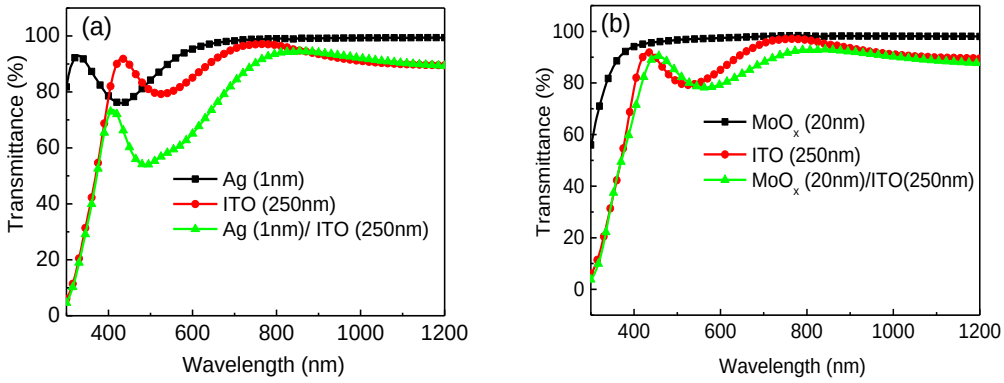

Figure 1. Transparency of the top ITO electrode with (a) 1nm Ag and (b) 20nm MoO_x

Aside from optical considerations, sputtered ITO is known to have poor adhesion to non-rigid substrates and low conductivity in the absence of high temperature treatment.[24-25] As such, the

effect of buffer layers on the deposition and growth of ITO are also critical factors to be examined. Sheet resistance of bare ITO, Ag/ITO and MoO_x/ITO are 29.96 ± 1.74 Ω/ square, 30.44 ± 0.83Ω/ square and 29.31 ± 0.49 Ω/ square respectively. Relatively similar sheet resistance can be observed at all sputtered ITO condition and may be due to the very thin buffer layers.

Although the conductivity is quite similar, severe ITO delamination on MoO_x is observed after exposure to ambient conditions as shown in the photograph of the complete devices (Figure 2a and 2b). FESEM cross section of complete device reveals ITO buckling delamination from the underlying layer (Figure 2c and 2d). This kind of buckling delamination can occur due to internal stress of the ITO layer.[24]

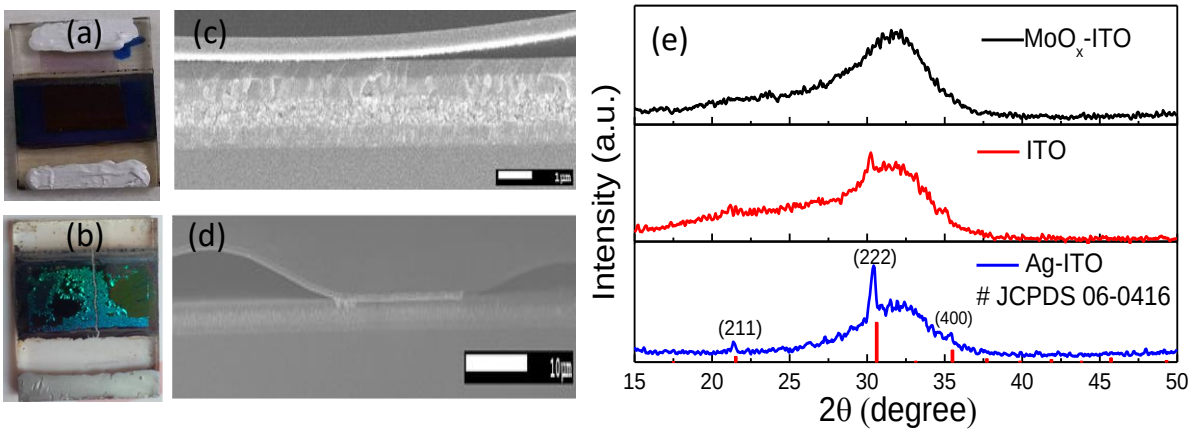

Figure 2. Digital photograph of semi-transparent device using ITO as top electrode with (a) 1 nm Ag buffer layer and (b) 20 nm MoO_x buffer layer which showing severe delamination of ITO, (c) and (d) cross-section SEM images of the device using MoO_x as buffer layer, it showed ITO was peeled off from the underneath layer with 1µm and 10µm magnification respectively, (e) XRD of sputtered ITO grown on different buffer layer. The amorphous hump originates from the underlying glass side.

As such, even though the utilization of MoO_x may result in better device bifacial performance due to lower parasitic absorption, MoO_x is known to be able to undergo redox reaction due to its sensitive nature toward oxygen in the environment, due to non-stoichiometry and presence of oxygen vacancies.[26-27] The physical properties of the MoO_x may have changed drastically and so may be a source of stress for deposited ITO.[24, 26] It has also been reported previously that amorphous ITO is less resistant to cracking than the crystalline ITO and also the large mismatch in physical and chemical properties between ITO and the underlying layer makes the ITO much more mechanically unstable.[24] We have measured the XRD spectra of ITO thin film along with the ITO thin films grown on thin Ag and MoO_x as shown in Figure 2e. From the XRD spectra, it is obvious that ITO film grown on MoO_x is almost amorphous in nature while in the case of thin Ag, it shows an obvious peak at 30.4°, which matches the standard ITO XRD spectra (JCPDS # 06-0416). This poor ITO crystallinity with of MoO_x together with possible stoichiometric changes in MoO_x may yield the kind of delamination and cracking observed.

For device fabrication, we adopted the triple cation based perovskite as many recent reports have found triple cation based perovskite solar cells to be more robust to fabrication condition and environment condition.[28] We used 5 wt% of Cs with respect to formamidinium (FA) and methylammonium (MA) with a stoichiometry $Cs_x(MA_{0.17}FA_{0.83})_{(100-x)}Pb(I_{0.83}Br_{0.17})_3$ for the fabrication of the devices. Semitransparent devices were fabricated by a standard solution processed method as described in the experimental methods section. A schematic of the semi-transparent device is shown in Figure 3a. The perovskite absorber layer is sandwiched in between titanium oxide (TiO_2) electron transport layer (ETL) and spiro-oMeTAD (HTL). Two transparent

conducting electrodes: commercially purchased fluorine doped tin oxide (FTO) and sputtered ITO are used as back and top contact respectively. The device is illuminated from the FTO side to minimize parasitic absorption from the HTL and top contacts. An identical device using opaque Au electrode was also fabricated for comparison.

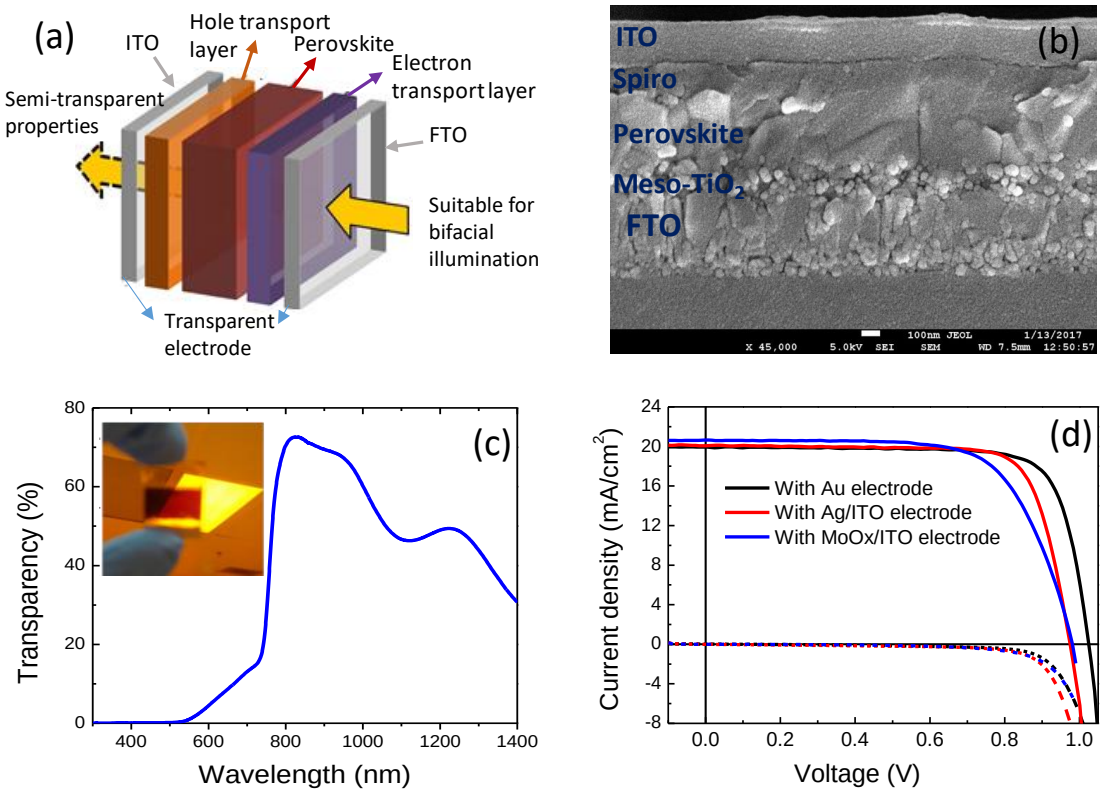

Figure 3. (a) Schematic of a semi-transparent device structure, (b) SEM cross-section of the device shows quite compact perovskite layer with thickness ~ 400 nm and uniform spiro layer with thickness ~150 nm and the top ITO electrode ~ 250 nm. (c) Transparency of the semitransparent device where Ag/ITO was taken as transparent electrode, inset shows the photograph of the semi-transparent device held against a room light. (d) Current-voltage (J-V) characteristics with a step size of 10 mV and scan velocity 250 mV/sec with opaque gold, Ag/ITO and MoO_x/ITO transparent electrodes.

Figure 3b shows the cross-section SEM image of a semi-transparent device. The thickness of the compact looking perovskite layer is ~ 400nm and the spiro-OMeTAD layer thickness of 150 nm. The full device stack shows an average transparency of 12% in the visible region and an average transparency of 54% from 800nm-1400nm (Figure 3c), comparable with previously reported semi-transparent perovskite solar cells.

Figure 3d shows the device performances of the semi-transparent cells along with the standard device with gold electrode measured under standard test condition (1sun, room temperature, RH ~70%) without any encapsulation. The standard device with gold electrode has an open circuit voltage (Voc) of 1025mV, short circuit current density (Jsc) of 19.9 mA/cm^2 and fill factor (FF) of 78.4%, which yields a power conversion efficiency (PCE) of 16.0%. Semi-transparent cells with Ag/ITO and MoO_x/ITO showed reduced performance with PCE of 15.3% and 13.8% respectively. Replacing the gold with the transparent ITO produced a drop in V_{OC} which could be indicative of increase interface recombination, while similar Jsc in all three devices indicates that the perovskite layer is sufficiently thick to harness all incident light. A significant drop in FF is observed when MoO_x buffer layer is used instead of Ag. While earlier sheet resistance measurement of ITO were comparable, the lower FF could be indicative of poorer vertical conductivity/recombination defects in MoO_x, or a result of ITO delamination not always obvious with MoO_x/ITO on glass but evident in a full solar cell device. The J-V parameters are summarized in Table 1.

Table 1.J-V comparison of perovskite solar cell using ITO and Au electrode

Electrode	J_{SC} (mA/cm^2)	V_{OC} (mV)	FF (%)	PCE (%)
Au	19.9	1025	78.4	16.0
Ag/ITO	20.1	975	78.1	15.3
MoO_x/ITO	20.6	981	68.4	13.8

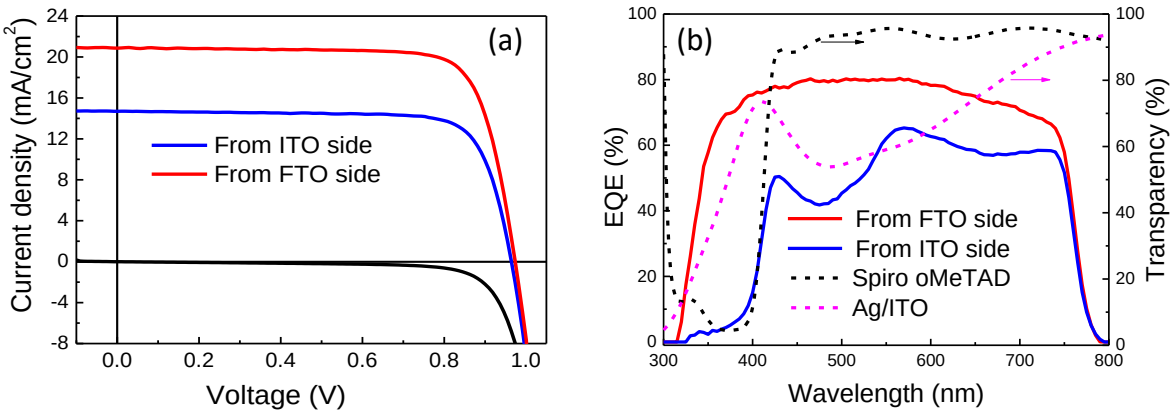

Figure 4. (a) J-V and (b) EQE of semi-transparent perovskite bifacial properties, transparency of the selected interlayers.

Although exhibiting good optical characteristics, poor adhesion of ITO and device performance found MoOx unsuitable for our purposes despite its popular use in literature. As seen in transparency measurements, the Ag/ITO stack's optical absorption and spiro-oMeTAD overlap with perovskite results in significant reduction of generated current when illuminated from the ITO side. Photocurrent reduction of ~6mA/cm2 was observed for illumination through ITO electrode and noted in the EQE (Figure 4), diminishing its effectiveness as a bi-facial device. This can be mollified with appropriate orientation, having the side with least parasitic absorption face the strongest light source when used in BIPV. For example, solar windows with the FTO/glass side facing outward would more efficiently collect strong external light. As perovskite solar cells are prone to have hysteresis effect, we checked the J-V characteristics of a semi-transparent device with Ag/ITO as electrode in forward and backward scan (as shown in Figure S3) and device showed no hysteresis effect. Regarding the stability of the device, we stored a device inside glovebox for 1 month and we found there is a drop of efficiency from 14.5% to 12.2% (as shown

in Table S1). We also checked the photo stability of the device by illuminating continuously for 30 min and we found an efficiency drop from 12.2% to 11.2% (as shown in Figure S4)

In the 4T tandem configuration, semi-transparent perovskite solar cell was electrically separated and mechanically stacked on top of low bandgap semiconductor solar cell (CIGS). The perovskite top cell acts as an optical filter on the CIGS cell and absorbs wavelength in between 300-800nm, while the unabsorbed higher wavelengths are harvested by the CIGS. An antireflection coating was used to the perovskite cell to minimize the optical loss. Individual cells were measured, and total tandem efficiency was obtained by the sum of both cells (Figure 5a).

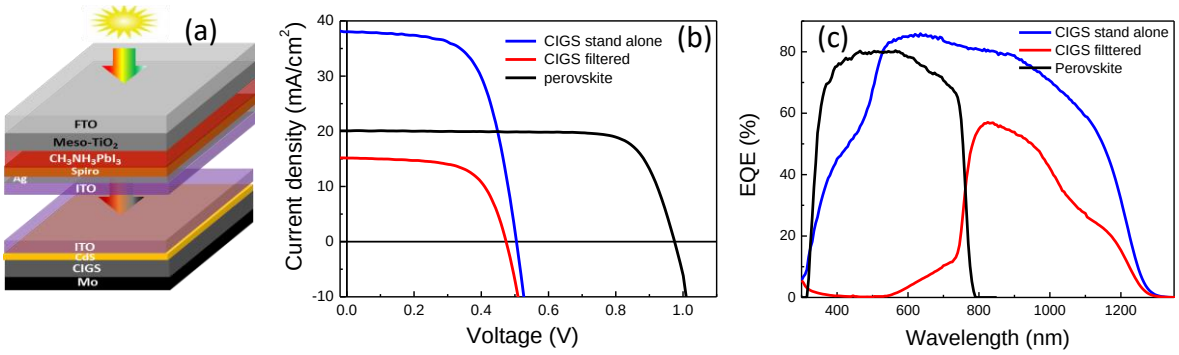

Figure 5. (a) Tandem schematic, (b) J-V curve, (c) EQE of 4-terminal tandem perovskite/CIGS combination

Table 2. J-V summary of 4-terminal tandem solar cells

Device	J_{sc} (mA/cm²)	V_{oc} (mV)	FF(%)	PCE (%)	PCE (%) with AR
Perovskite top cell	20.1	975	78.1	15.3	16.0
CIGS stand alone	38.0	509	63.8	12.3	
CIGS filtered	15.2	470	64.6	4.6	4.7
4-terminal tandem				19.9	20.7

The J-V curve and EQE of perovskite and CIGS cells before and after filtering are shown in Figure 5b, and the photovoltaic parameter summarized in Table 2. When the CIGS was filtered by perovskite, a slight drop of CIGS Voc was observed as a result of low intensity illumination. Significant decrease in Jsc brought down the overall PCE of CIGS from 12.3% (unfiltered) to 4.7% (filtered). This effect can be seen clearly in the external quantum efficiency (EQE) (Figure 5c). Combined with our optimized 16% semi-transparent perovskite, a total power conversion efficiency of 20.7% was obtained in this 4T configuration, showing an absolute efficiency exceeding the individual efficiencies of the subcells. For this 4T configuration, overall transparency of the top peroskite cells is very important. We found that our perovskite top cell has an average transparency of 54% in the region from 800 nm to 1400 nm, where the bottom CIGS cell has significant absorption. The transmission of the top perovskite cell increases rapidly from 700 nm and remain as high as 65% up to 1000 nm. After 1000 nm, transmission of the top cell decreases due to parasitic absorption by the electrodes which could be improved further by process. An airgap exists between the perovskite and CIGS cell, as such some optical loss due to reflection at the top interface of both cells are expected, but this effect was not characterized. To minimize reflection loss, any index matched material could be useful to couple transmitted light into the bottom cell.

In conclusion, we demonstrate a 16% efficiency of triple cation semi-transparent perovskite solar cell along with more than 12% transparency in visible light range and more than 50% transparency in the near infrared region. Proper comparative studies on different buffer layer prior to the deposition of transparent sputtered ITO revealed the advantages of thermal evaporated thin Ag buffer layer as compared to amorphous MoO_x, as mostly indicated by improved adhesion to the

under layer and a better FF which yields higher power conversion efficiencies. By using this optimized perovskite cell, a 4T tandem perovskite/CIGS solar cell with 20.7% efficiency (device efficiency is not certified yet) and an absolute efficiency improvement of more than 7% as compared to single junction CIGS cell was realized.

EXPERIMENTAL METHODS

SEMI-TRANSPARENT PEROVSKITE DEVICE FABRICATION

Fluorine doped tin oxide (FTO) glass substrates (Tec15) were cleaned by ultra-sonication in a decon soap solution followed by deionized water and ethanol. The cleaned substrates were then treated under UV ozone for 15min prior to usage. Compact TiO_2 (c-TiO_2) was spray deposited at 500°C on a sintering hotplate, using titanium diisopropoxide bis (acetylacetonate) (Sigma-Aldrich, 75 wt% in isopropanol) mix with isopropanol (Sigma Aldrich, anhydrous) and acethylacetone (Sigma Aldrich). For the Mesoporous TiO_2 (mp-TiO_2) layer, Dyesol 30NRD was diluted in absolute ethanol in the ratio 1:5.5 (w/w) and then spun onto the substrate at 5500 rpm for 30s. The substrate was then sintered at 500°C for 15 min. Before device fabrication, 10mg/mL lithium bis(trifluoromethylsulphonyl) imide solution in acetonitrile (Sigma Aldrich, anhydrous)was spun on at 3000rpm for 20s and annealed at 450°C for 30 min

1.35M triple cation perovskite precursor solution, $Cs_{0.05}(MA_{0.17}FA_{0.83})_{0.95}Pb(I_{0.83}Br_{0.17})_3$, was prepared by dissolving MABr (Dyesol), $PbBr_2$ (TCI), FAI (Dyesol), PbI_2 (TCI) inside a mixture of DMF and DMSO with a ratio of 4:1 (v/v) at room temperature for 1h. CsI in DMSO was added into the perovskite precursor solution to form the composition required. The dissolved perovskite solution was spin-coated on mp-TiO_2 layer first at 1000 rpm for 10 sec followed immediately by

6000rpm for 17s. Simultaneously, 0.1mL dichlorobenzene was dripped onto the substrate at 13s. The film was then heated at 100°C for 1h in order to obtain black and dense perovskite film. On top of the perovskite layer, a solution of spiro-OMeTAD (70mg/mL in chlorobenzene), with addition of 4-*tert*-butylpyridine, lithium bis(trifluoromethylsulphonyl) imide (520mg/mL in acetonitrile (ACN)) and FK102 (17.2mg/50 mL of ACN) was spin-coated at 5000rpm for 30s. All the perovskite and HTM preparations were done inside glovebox.

Gold back contact (100nm) was deposited using thermal evaporation for opaque perovskite device. While for semi-transparent perovskite device, 250nm indium tin oxide (ITO) was deposited using DC sputter at 25W power for 1 hour, to form a transparent electrode. The Ar and O_2 gas flow rate was 30 and 0.6 sscm respectively. Prior ITO deposition, a buffer layer of thin Ag or MoO_x, was posited through thermal evaporation. Where indicated, an antireflection film was applied to the glass side of the device.

CIGS DEVICE FABRICATION

CIGS approximately 1um thick was deposited via vacuum sputtering method onto Molybdenum coated glass. Next, a 60nm buffer layer of Cadmium Sulfide (CdS) was deposited using chemical bath deposition (CBD) at 80^{o}C. For the transparent top contact, 250 nm of ITO was sputtered deposited at ambient temperature. Finally, the device was annealed in a 2-zone tube furnace at 300^{o}C for 10 mins. The completed device was mechanically scribed to produce individual cells with dimension 0.4 x 0.4cm.

THIN FILM AND DEVICE CHARACTERIZATIONS

Transmission (T) spectra of the thin films were recorded using UV-Vis-NIR Spectrophotometer (UV3600, Shimadzu) equipped with an integrating sphere from 300-1200nm wavelength. Top

view and cross section images of the devices were recorded using a Field Emission Scanning Electron Microscope (FESEM, JEOL, JSM-7600F, 5kV and 10mA). A thin layer of Pt was coated on top of the samples to avoid charging effect. Thin films were also characterized by X-ray diffraction (Bruker D8 Advance). Photocurrent-voltage characteristics of both perovskite and CIGS solar cells were recorded by applying an external potential bias to the cells while recording the generated photocurrent with a digital dial source meter (Keithley 2612 sourcemeter). The J-V measurements were measured using San-EI Electric, XEC-301S solar simulator under standard simulated AM1.5G illumination and the light intensity was calibrated using standard reference silicon cell. The incident photon to current conversion efficiency (IPCE) was determined using a PVE300 (Bentham), with a dual xenon/quartz halogen light source and measured in DC mode without additional light bias. The light intensity was calibrated using a silicon calibrated detector (Newport). An aperture mask with dimensions 0.3x0.3 cm was used for Perovkite J-V and tandem measurements.

ASSOCIATED CONTENT

Supporting Information. Optical transparency, preliminary solar cells results, hysteresis study and photo stability study

AUTHOR INFORMATION

Corresponding Author

*Email: Nripan@ntu.edu.sg

Notes

The authors declare no competing financial interest.

ACKNOWLEDGMENT

This research is supported by the National Research Foundation, Prime Minister's Office, Singapore under its Campus for Research Excellence and Technological Enterprise (CREATE) programme, Singapore -Berkeley Research Initiative for Sustainable Energy (SinBeRISE). Funding from NTU-A*STAR Silicon Technologies Centre of Excellence under the program grant No. 112 3510 0003 and MOE Tier 1 grant RG184/14 is also acknowledged.

REFERENCES:

(1) Service, R. F. Perovskite Solar Cells Gear up to go Commercial. *Science* **2016,** *354*, 1214-1215.

(2) Stranks, S. D.; Snaith, H. J. Metal-Halide Perovskites for Photovoltaic and Light-Emitting Devices. *Nat. Nanotechnol.* **2015,** *10*, 391-402.

(3) Snaith, H. J. Perovskites: The Emergence of a New Era for Low-Cost, High-Efficiency Solar Cells. *J. Phys. Chem. Lett.* **2013,** *4*, 3623-3630.

(4) Werner, J.; Barraud, L.; Walter, A.; Bräuninger, M.; Sahli, F.; Sacchetto, D.; Tétreault, N.; Paviet-Salomon, B.; Moon, S.-J.; Allebé, C.; *et al.*. Efficient Near-Infrared-Transparent Perovskite Solar Cells Enabling Direct Comparison of 4-Terminal and Monolithic Perovskite/Silicon Tandem Cells. *ACS Energy Lett.* **2016,** *1*, 474-480.

(5) Albrecht, S.; Saliba, M.; Correa Baena, J. P.; Lang, F.; Kegelmann, L.; Mews, M.; Steier, L.; Abate, A.; Rappich, J.; Korte, L.; *et al.* Monolithic Perovskite/Silicon-Heterojunction Tandem Solar Cells Processed at Low Temperature. *Energy Environ. Sci.* **2016,** *9*, 81-88.

(6) Fu, F.; Feurer, T.; Weiss, Thomas P.; Pisoni, S.; Avancini, E.; Andres, C.; Buecheler, S.; Tiwari, Ayodhya N. High-Efficiency Inverted Semi-Transparent Planar Perovskite Solar Cells in Substrate Configuration. *Nat. Energy.* **2016,** *2*, 16190.

(7) NREL, Best Research Cell Efficiencies, https://www.nrel.gov/pv/assets/images/efficiency-chart.png (2016).

(8) Zhou, H.; Chen, Q.; Li, G.; Luo, S.; Song, T.-b.; Duan, H.-S.; Hong, Z.; You, J.; Liu, Y.; Yang, Y. Interface Engineering of Highly Efficient Perovskite Solar Cells. *Science* **2014,** *345*, 542-546.

(9) Bi, D.; Tress, W.; Dar, M. I.; Gao, P.; Luo, J.; Renevier, C.; Schenk, K.; Abate, A.; Giordano, F.; Correa Baena, J.-P.; Decoppet, J.-D.; *et al.* Efficient Luminescent Solar Cells Based on Tailored Mixed-Cation Perovskites. *Sci. Adv.* **2016,** *2*, e1501170.

(10) Stranks, S. D.; Eperon, G. E.; Grancini, G.; Menelaou, C.; Alcocer, M. J. P.; Leijtens, T.; Herz, L. M.; Petrozza, A.; Snaith, H. J. Electron-Hole Diffusion Lengths Exceeding 1 Micrometer in an Organometal Trihalide Perovskite Absorber. *Science* **2013,** *342*, 341-344.

(11) Werner, J.; Dubuis, G.; Walter, A.; Löper, P.; Moon, S.-J.; Nicolay, S.; Morales-Masis, M.; De Wolf, S.; Niesen, B.; Ballif, C. Sputtered Rear Electrode with Broadband Transparency for Perovskite Solar Cells. *Sol. Energ. Mat. Sol. Cells* **2015,** *141*, 407-413.

(12) Werner, J.; Weng, C.-H.; Walter, A.; Fesquet, L.; Seif, J. P.; De Wolf, S.; Niesen, B.; Ballif, C. Efficient Monolithic Perovskite/Silicon Tandem Solar Cell with Cell Area >1 cm2. *J. Phys. Chem. Lett.* **2016,** *7*, 161-166.

(13) McMeekin, D. P.; Sadoughi, G.; Rehman, W.; Eperon, G. E.; Saliba, M.; Hörantner, M. T.; Haghighirad, A.; Sakai, N.; Korte, L.; Rech, B.; *et al.* Mixed-Cation Lead Mixed-Halide Perovskite Absorber for Tandem Solar Cells. *Science* **2016,** *351*, 151-155.

(14) Eperon, G. E.; Leijtens, T.; Bush, K. A.; Prasanna, R.; Green, T.; Wang, J. T.-W.; McMeekin, D. P.; Volonakis, G.; Milot, R. L.; May, R.; *et al.* Perovskite-Perovskite Tandem Photovoltaics with Optimized Bandgaps. *Science* **2016**, DOI: 10.1126/science.aaf9717.

(15) Fu, F.; Feurer, T.; Jäger, T.; Avancini, E.; Bissig, B.; Yoon, S.; Buecheler, S.; Tiwari, A. N. Low-Temperature-Processed Efficient Semi-Transparent Planar Perovskite Solar Cells for Bifacial and Tandem Applications. *Nat. Commun.* **2015,** *6*, 8932.

(16) Guo, F.; Azimi, H.; Hou, Y.; Przybilla, T.; Hu, M.; Bronnbauer, C.; Langner, S.; Spiecker, E.; Forberich, K.; Brabec, C. J. High-Performance Semitransparent Perovskite Solar cells with Solution-Processed Silver Nanowires as Top Electrodes. *Nanoscale* **2015,** *7*, 1642-1649.

(17) You, P.; Liu, Z.; Tai, Q.; Liu, S.; Yan, F. Efficient Semitransparent Perovskite Solar Cells with Graphene Electrodes. *Adv. Mater.* **2015,** *27*, 3632-3638.

(18) Bailie, C. D.; Christoforo, M. G.; Mailoa, J. P.; Bowring, A. R.; Unger, E. L.; Nguyen, W. H.; Burschka, J.; Pellet, N.; Lee, J. Z.; Gratzel, M.; *et al.* . Semi-Transparent Perovskite Solar Cells for Tandems with Silicon and CIGS. *Energy Environ. Sci.* **2015,** *8*, 956-963.

(19) Bush, K. A.; Bailie, C. D.; Chen, Y.; Bowring, A. R.; Wang, W.; Ma, W.; Leijtens, T.; Moghadam, F.; McGehee, M. D. Thermal and Environmental Stability of Semi-Transparent Perovskite Solar Cells for Tandems Enabled by a Solution-Processed Nanoparticle Buffer Layer and Sputtered ITO Electrode. *Adv. Mater.* **2016,** *28*, 3937-3943.

(20) Lee, M.; Jo, Y.; Kim, D. S.; Jeong, H. Y.; Jun, Y. Efficient, Durable and Flexible Perovskite Photovoltaic Devices with Ag-Embedded ITO as the Top Electrode on a Metal Substrate. *J. Mater. Chem. A* **2015,** *3*, 14592-14597.

(21) Lang, F.; Nickel, N. H.; Bundesmann, J.; Seidel, S.; Denker, A.; Albrecht, S.; Brus, V. V.; Rappich, J.; Rech, B.; Landi, G.; Neitzert, H. C. Radiation Hardness and Self-Healing of Perovskite Solar Cells. *Adv. Mater.* **2016,** *28*, 8726-8731.

(22) Jasenek, A.; Schock, H. W.; Werner, J. H.; Rau, U. Defect Annealing in Cu(In,Ga)Se2 Heterojunction Solar Cells after High-Energy Electron Irradiation. *Appl. Phys. Lett.* **2001,** *79*, 2922-2924.

(23) Guillemoles, J.-F.; Rau, U.; Kronik, L.; Schock, H.-W.; Cahen, D. Cu(In,Ga)Se2 Solar Cells: Device Stability Based on Chemical Flexibility. *Adv. Mater.* **1999,** *11*, 957-961.

(24) Kim, E.-H.; Yang, C.-W.; Park, J.-W. The Crystallinity and Mechanical Properties of Indium Tin Oxide Coatings on Polymer Substrates. *J. Appl. Phys.* **2011,** *109*, 043511-043511-8.

(25) Porter, G. A.; Chao, C. K.; Chang, R. C.; Li, Y. C. Effects of Different Interlayers on Indium-Tin Oxide Thin Films Sputtered on Flexible PET Substrates. *J. Chinese Inst. Engrs.* **2011,** *34*, 549-557.

(26) Irfan, I.; Gao, Y. Effects of Exposure and Air Annealing on MoOx Thin Films. *J. Photon. Energy.* **2012,** *2*, 021213-1-021213-12.

(27) Werner, J.; Geissbühler, J.; Dabirian, A.; Nicolay, S.; Morales-Masis, M.; Wolf, S. D.; Niesen, B.; Ballif, C. Parasitic Absorption Reduction in Metal Oxide-Based Transparent

Electrodes: Application in Perovskite Solar Cells. *ACS Appl. Mater. Interfaces* **2016,** *8*, 17260-17267.

(28) Saliba, M.; Matsui, T.; Seo, J.-Y.; Domanski, K.; Correa-Baena, J.-P.; Nazeeruddin, M. K.; Zakeeruddin, S. M.; Tress, W.; Abate, A.; Hagfeldt, A.; *et al.* . Cesium-Containing Triple Cation Perovskite Solar Cells: Improved Stability, Reproducibility and High Efficiency. *Energy Environ. Sci.* **2016,** *9*, 1989-1997.